Internal nanoparticle structure of temperature-responsive self-assembled PNIPAM-b-PEG-b-PNIPAM triblock copolymers in aqueous solutions: NMR, SANS and light scattering studies

Article

Published Version

Open Access

Filippov, S. K., Bogomolova, A., Kaberov, L., Velychkivska, N., Starovoytova, L., Cernochova, Z., Rogers, S. E., Lau, W. M., Khutoryanskiy, V. V. ORCID: https://orcid.org/0000-0002-7221-2630 and Cook, M. T. (2016) Internal nanoparticle structure of temperature-responsive self-assembled PNIPAM-b-PEG-b-PNIPAM triblock copolymers in aqueous solutions: NMR, SANS and light scattering studies. Langmuir, 32 (21). pp. 5314-5323. ISSN 1520-5827 doi: https://doi.org/10.1021/acs.langmuir.6b00284 Available at https://centaur.reading.ac.uk/65646/

www.reading.ac.uk/centaur

CentAUR

Central Archive at the University of Reading

Reading's research outputs online

LANGMUIR

Internal Nanoparticle Structure of Temperature-Responsive Self-Assembled PNIPAM-*b*-PEG-*b*-PNIPAM Triblock Copolymers in Aqueous Solutions: NMR, SANS, and Light Scattering Studies

Sergey K. Filippov,*,[†] Anna Bogomolova,[†] Leonid Kaberov,[†] Nadiia Velychkivska,[†] Larisa Starovoytova,[†] Zulfiya Cernochova,[†] Sarah E. Rogers,[‡] Wing Man Lau,[∥] Vitaliy V. Khutoryanskiy,[∥] and Michael T. Cook*,[⊥]

[†]Institute of Macromolecular Chemistry, AS CR, Heyrovsky Sq. 2, Prague, Prague 6, 162 06, Czech Republic

[‡]ISIS-STFC, Rutherford Appleton Laboratory, Chilton, OX11 0QX Oxon United Kingdom

[∥]School of Pharmacy, University of Reading, Whiteknights, PO Box 224, Reading, RG6 6AD Berkshire, United Kingdom

[⊥]Department of Pharmacy & Research Centre in Topical Drug Delivery and Toxicology, University of Hertfordshire, Hatfield, AL10 9AB Hertfordshire, United Kingdom

S *Supporting Information*
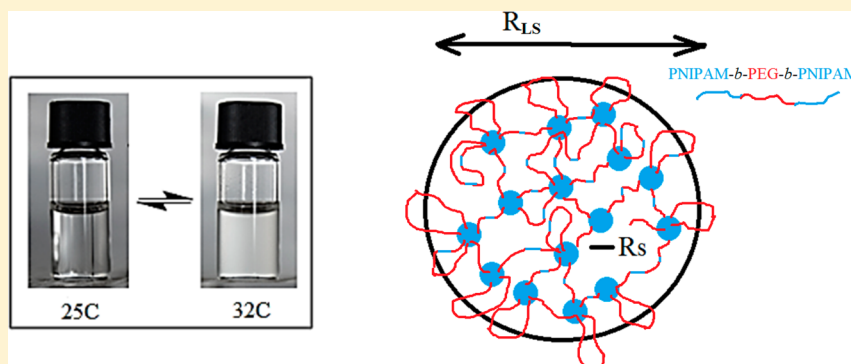
ABSTRACT: In this study, we report detailed information on the internal structure of PNIPAM-*b*-PEG-*b*-PNIPAM nanoparticles formed from self-assembly in aqueous solutions upon increase in temperature. NMR spectroscopy, light scattering, and small-angle neutron scattering (SANS) were used to monitor different stages of nanoparticle formation as a function of temperature, providing insight into the fundamental processes involved. The presence of PEG in a copolymer structure significantly affects the formation of nanoparticles, making their transition to occur over a broader temperature range. The crucial parameter that controls the transition is the ratio of PEG/PNIPAM. For pure PNIPAM, the transition is sharp; the higher the PEG/PNIPAM ratio results in a broader transition. This behavior is explained by different mechanisms of PNIPAM block incorporation during nanoparticle formation at different PEG/PNIPAM ratios. Contrast variation experiments using SANS show that the structure of nanoparticles above cloud point temperatures for PNIPAM-*b*-PEG-*b*-PNIPAM copolymers is drastically different from the structure of PNIPAM mesoglobules. In contrast with pure PNIPAM mesoglobules, where solidlike particles and chain network with a mesh size of 1−3 nm are present, nanoparticles formed from PNIPAM-*b*-PEG-*b*-PNIPAM copolymers have nonuniform structure with "frozen" areas interconnected by single chains in Gaussian conformation. SANS data with deuterated "invisible" PEG blocks imply that PEG is uniformly distributed inside of a nanoparticle. It is kinetically flexible PEG blocks which affect the nanoparticle formation by prevention of PNIPAM microphase separation.

■ INTRODUCTION

Temperature-responsive polymers are a class of materials which undergo phase changes upon heating or cooling their solutions. If a polymer displays an expanded coil to globule transition during heating, associated with reduced solubility, it is said to display a cloud point temperature (CPT). A phase diagram for aqueous solutions of temperature-responsive polymers is characterized by a so-called lower critical solution temperature (LCST).[1,2] This transition occurs due to an unfavorable entropy of mixing. A polymer reaching its CPT is usually associated with an increase in solution turbidity due to the collapse of the expanded coil, resulting in a globule which is able to phase separate via a mesoglobular state, which subsequently scatters light. For a homopolymer, the final result

of reaching the CPT is polymer phase separation in solution. In block copolymer solutions, however, the phase separation of one block can result in the formation of a self-assembled structure, including micelles,[3−10] wormlike micelles,[11] and gels.[12] These self-assembled structures have potential use in drug delivery, releasing their load in a temperature-dependent fashion.[13]

Poly(N-isopropylacrylamide) (PNIPAM) is one of the most highly studied temperature-responsive polymers exhibiting a LCST. The LCST of a PNIPAM homopolymer is approximately 32 °C, though copolymerization with hydrophilic monomers may alter this, as well as changes in concentration, ionic strength, and pH.[14] Diblock copolymers of poly(ethylene glycol) (PEG) and PNIPAM are able to form micelles,[15−18] vesicles,[19,20] and gels,[21,22] depending on molecular weights and concentration. It was established that vesicles are formed from a three-level intermediate hierarchical structure that exist in solution below CPT.[20] ABA triblock copolymers of PNIPAM-b-PEG-b-PNIPAM have been less studied,[22,23] and are known to form both micelles[15] and gels.[21,22] At high concentrations of block copolymer (>20 wt %), gels are formed, depending on the molecular weight of each block.[21] At lower concentrations, shorter block length is detrimental to gel formation. Topp et al.[15] used cerium to initiate chain growth of PNIPAM (1.6 kDa) from PEG (6 kDa) to give ABA triblock copolymers which assembled into micelles above 30.9 °C. This was not an extensive study, but to our knowledge is the first report of these materials. However, the effect of molecular weight of each block was not determined. Previously, Hennik et al.[23] studied PNIPAM-b-PEG-b-PNIPAM copolymers and the presence of flowerlike micelles in solution was reported above CPT in contrast with ordinary micelles formed by PEG-b-PNIPAM copolymers. Existence of loops in flowerlike micelles was convincingly demonstrated by ^{1}H NMR relaxometry.[23]

In this study, we use small-angle neutron scattering (SANS), light scattering, and NMR to study the formation of nanoparticles from PNIPAM-b-PEG-b-PNIPAM block copolymers. The main difference of PNIPAM-b-PEG-b-PNIPAM block copolymers reported here from ones reported in refs 19, 20, and 23 is much shorter length of PNIPAM block. This allows for comprehensive study of the internal structure of these self-assembled nanostructures, as well as the other features occurring during self-assembly.

■ EXPERIMENTAL SECTION

Materials. Tris(2-aminoethyl)amine (TREN), polyethylene glycol (PEG, 4 kDa), α-bromoisobutyryl bromide (BIBB), formic acid, formaldehyde, N-isopropylacrylamide (NIPAM), and copper(I) chloride were purchased from Sigma-Aldrich (U.K.). Deuterated PEG (3.5 kDa) was purchased from Polymer Source (Canada). Dialysis membranes with a 3.5 kDa molecular weight cutoff (MWCO) were purchased from Visking (U.K.) and soaked for 1 h in deionized water prior to use. Toluene and triethylamine were dried over 3 Å molecular sieves for 24 h prior to use.

Methods. *Synthesis of PNIPAM-b-PEG-b-PNIPAM Triblock Copolymers via Atom-Transfer Radical-Polymerization (ATRP).* ATRP was conducted using the difunctionalized PEG macroinitiator and ME₆TREN catalyst described in Supporting Information, with an initiator/catalyst/ligand ratio of 1:1:1. The ATRP procedure was as follows: CuCl (12.4 mg, 125 μmol) was placed into a round-bottom flask, sealed with a septum, then purged with N₂ for 20 min. A second flask was prepared containing NIPAM (500 mg for "low" MW PNIPAM or 1.25 g for "high" MW PNIPAM) and PEG macroinitiator (500 mg, 125 μmol). H₂O (2 mL) was added, followed by Me₆TREN (33.4 μL, 28.8 mg, 125 μmol). The solution was then allowed to stir at

room temperature until complete dissolution (ca. 5 min). The solution containing NIPAM, macroinitiator, and ligand was then bubbled through with N₂ for 20 min, at which point it was transferred to the flask containing CuCl via syringe. The reaction was then allowed to proceed at room temperature for 24 h with stirring. The resulting blue-green solution was concentrated in vacuo, dissolved in tetrahydrofuran (THF) (5 mL), and then passed through a short length of neutral alumina, resulting in a colorless solution. This was concentrated in vacuo to yield a white solid, PNIPAM-b-PEG-b-PNIPAM. Dialysis (MWCO 3.5 kDa) was necessary to remove residual monomers (as detected by ^{1}H NMR). ^{1}H NMR (400 MHz, D₂O, δ): 3.86 (br, CH PNIPAM), 3.66 (br, CH₂ PEG), 1.97 (br, CH₂ PNIPAM), 1.54 (br, CH₂ PNIPAM), 1.11 (br, CH₃ PNIPAM) ppm.

Gel Permeation Chromatography (GPC). GPC was conducted in order to determine polydispersity indexes (PDIs) and confirm that PEG and PNIPAM blocks were bonded to each other. An Agilent 1260 Infinity GPC-SEC system combined with 1 x Waters Styragel HR2 column was used. THF was used as mobile phase at a flow rate of 1.0 mL min⁻¹. Polystyrene standards and samples were dissolved in THF (2 mg/mL) with gentle heating to ensure complete dissolution of PEG. M_n values quoted are determined by relative, narrow standard, calibration.

Nuclear Magnetic Resonance (NMR). To characterize the behavior of the polymer system, the ^{1}H and ^{1}H spin−spin relaxation times T_2 were measured using NMR spectroscopy. Relaxation NMR spectroscopy is a useful tool for investigating polymer and solvent dynamics due to the fact that the transverse magnetization component is sensitive to changes in the mobility of polymer segments as well as the solvent.[10,24−26]

^{1}H NMR measurements were performed with a Bruker Avance III 600 spectrometer operating at 600.2 MHz. The integrated intensities were determined with the spectrometer integration software at an accuracy of ±1%. In all measurements, the temperature was maintained at a constant value within ±0.2 °C using a BVT 3000 temperature unit. The samples were kept at the experimental temperature for at least 15 min before the measurement. The measurement conditions were as follows: 90 pulses with a width of 10 μs, relaxation delay of 10 s, spectral width of 4844.961 Hz, and 8 scans in the temperature range 17−57 °C. The ^{1}H spin−spin relaxation times T_2 for all components were measured using the CPMG pulse sequence $90°x−(t_d−180°y−t_d)_n$-acquisition with t_d = 0.5 ms. Each experiment was conducted with four scans, a relaxation delay of 80 s, and a spectral width of 9014.423 Hz. The obtained T_2 relaxation curves were monoexponential and the fitting process made it possible to determine a single value of the relaxation time. The relative error for T_2 values of PNIPAM, HDO, and PEG protons did not exceed ±8%, ±5%, and ±6%, respectively.

To quantitatively characterize the phase separation, we have used the values of the phase-separated fraction p obtained as

$$p(T) = 1 - \frac{I}{I_0} \tag{1}$$

where I is the integrated intensity of the given polymer signal in the spectrum of the partly separated system and I_0 is the integrated intensity of this signal if no phase separation occurs. For I_0, we took values based on integrated intensities below the phase transition, using the expected $1/T$ temperature dependence. The integrated intensities were measured ∼20 min after the corresponding temperature was reached (by heating).

Small-Angle Neutron Scattering (SANS). SANS experiments were performed on the time-of-flight Sans2d diffractometer at the ISIS neutron facility, U.K. A simultaneous Q-range of 0.005−0.85 Å⁻¹ was achieved by utilizing an incident wavelength range of 1.75−16.5 Å and employing an instrument setup of $L_1 = L_2 = 4$ m with the detector offset vertically 75 mm and sideways 305 mm. The beam diameter was 8 mm. Each scattering data set was corrected for the detector efficiencies, sample transmission and background scattering and converted to scattering cross section data using instrument specific software.[27] These data were placed on an absolute scale (cm⁻¹) using
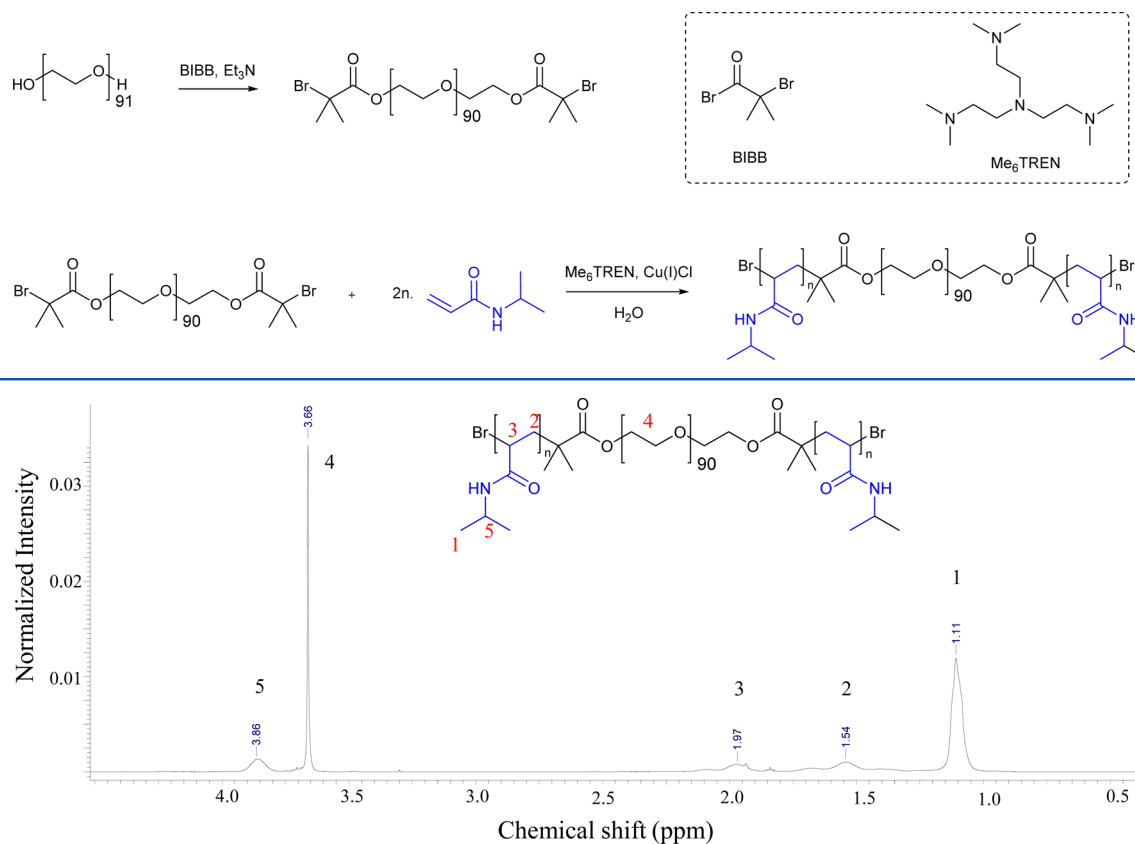
Scheme 1. Synthetic Route to PNIPAM-*b*-PEG-*b*-PNIPAM Triblock Copolymers

Figure 1. Exemplar ^{1}H NMR of PNIPAM-*b*-PEG-*b*-PNIPAM, displaying characteristic peaks of both PEG and PNIPAM.

Table 1. Molecular Weight and PDI of PNIPAM-*b*-PEG-*b*-PNIPAM Triblock Copolymers

sample ID	M_n (kDa)	PDI	M_n of PEG (kDa, manufacturer)	M_n of PNIPAM blocks (kDa) GPC	N of PNIPAM blocks	N of PEG blocks
A	10.3	1.4	3.5^b	3.4	30	79
B	12.5	1.3	4.0	4.3	38 (43^a)	90
C	15.8	1.2	3.5^b	6.2	54	79
D	15.5	1.2	4.0	5.8	51 (60^a)	90

^{a}Data from NMR in D$_2$O. ^{b}PEG is deuterated.

the scattering from a standard sample (a solid blend of hydrogenous and perdeuterated polystyrene) in accordance with established procedures.[28] All solutions for SANS experiments were prepared using D$_2$O as solvent to reduce incoherent scattering. The concentrations of all solutions was 0.5 wt %. Scattering from pure D$_2$O was measured separately and subtracted from solution scattering data.

Light Scattering. Static and dynamic light scattering (SLS and DLS) was performed to characterize the micelles in dilute solutions. Initially, the pH dependency of the hydrodynamic radius of particles, R_h, and the scattering intensity, I_s, were measured at a scattering angle of $\theta = 173°$ with a Zetasizer Nano-ZS instrument, model ZEN3600 (Malvern Instruments, U.K.). The DTS (Nano) program was used to evaluate the data. It provides intensity-, volume-, and number-weighted R_h distribution functions $G(R_h)$.[29] The intensity-weighted value of the apparent R_h was chosen to monitor the temperature-dependent changes in the system.

Static Light Scattering. The static light scattering measurements were performed at 40 °C in the angular range 40−140° using an ALV goniometer equipped with a 30 mW He−Ne laser ($\lambda = 632.8$ nm). Data evaluation was carried out through using Guinier and Berry models.[30] The differential index of refraction (dn/dc) was determined in a BI-DNDCW differential refractometer (Bruckhaven Instruments Corporation) at 620.0 nm, with Differential Refractometer Software.

Stock solutions of PNIPAM-*b*-PEG-*b*-PNIPAM copolymers were prepared in D$_2$O (1 g/dm^3). The dn/dc value was found to be around 1.45×10^{-4} L/g.

3D-DLS. The aforementioned system is relatively turbid, denoting the existence of multiple scattering contributions. Therefore, the undesired multiple scattering contributions should be suppressed in order to get reliable measurements of the form factor, in diluted solutions, or of the structure factor in more concentrated ones.[31−33] Thus, the 3D-DLS cross-correlation technique was used where the scattering intensity from two beams of the same wavelength corresponding to the same scattering vector, but different scattering planes on the same scattering volume are cross-correlated. It has been shown that contributions from multiple scattering events is eliminated in this way, enabling us to extract information on only the single scattering contribution. The experimental setup which was used for both DLS and SLS measurements is the 3D LS spectrometer from LS instruments consisting of a goniometer system equipped with a single laser beam (Lumentum 1145/P HeNe laser 21 mW) at 632.8 nm. Experiments were conducted at 40 °C.

■ RESULTS AND DISCUSSION

PNIPAM-*b*-PEG-*b*-PNIPAM triblock copolymers were synthesized using ATRP polymerization from a difunctionalized PEG

macroinitiator (Scheme 1). This synthesis was conducted in aqueous conditions, using ME$_6$TREN as a ligand for a copper(I) chloride catalyst, which has been reported for the polymerization of PNIPAM.[34] Oxidation of copper(I) to copper(II) during the polymerization leads to the appearance of a blue-green color solution, which was removed by passage through a short length of neutral alumina. ^{1}H NMR (Figure 1) showed that polymerization had occurred, with vinylic protons of the acrylamide moiety not present, replaced with alkyl protons at 1.97 and 1.54 ppm, corresponding to the polymer backbone. Additional characteristic broad peaks were identified for PNIPAM at 3.86 (CH) and 1.11 (CH$_3$) ppm, as well as the CH$_2$ protons for PEG at 3.66 ppm.

Four samples were produced in total, in which the PEG blocks were either deuterated or nondeuterated, with PNIPAM blocks of two different molecular weights as determined by GPC (Table 1). These four samples can be grouped into two pairs. **A** and **B** have matched molecular weight deuterated-PEG and PEG blocks (3.5 and 4 kDa, respectively) and "short" PNIPAM blocks (3.4 and 4.3 kDa, respectively). **C** and **D** have matched molecular weight deuterated-PEG and PEG blocks (3.5 and 4 kDa, respectively) and "long" PNIPAM blocks (6.2 and 5.8 kDa, respectively). All products had satisfactory PDIs (<1.4), considering the polydispersities of the macroinitiators.[34]

Dynamic light scattering experiments directly prove the presence of nanoparticles in solution at high temperature (Figure 2). A sharp transition is seen at the CPT of PNIPAM
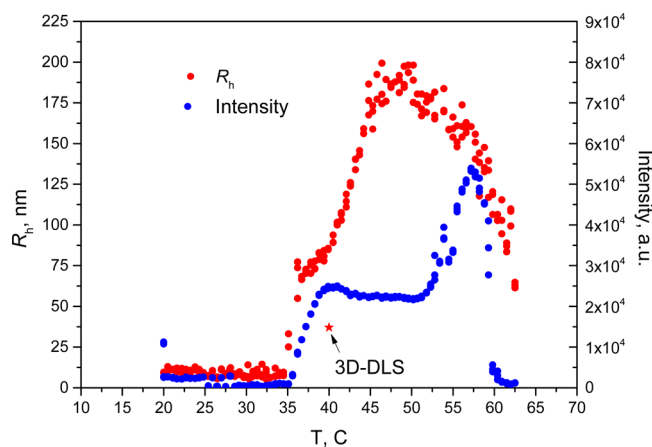

Figure 2. Temperature dependence of apparent hydrodynamic radius and scattered intensity for sample **D** measured using conventional DLS at c = 1.0 wt %. Star point indicated by arrow is the hydrodynamic radius value measured by 3D-DLS method.

(approximately 35 °C), resulting in the formation of nanoparticles with a hydrodynamic radius (R_h) of approximately 75 nm. It should be noted here that a low fraction of 200−300 nm aggregates was seen at low temperatures. This peak was discarded in Figure 2 due to concentration of these aggregates in solution is negligible. Above the CPT, the distribution was monomodal.

Further heating above CPT results in continuous increase in the apparent hydrodynamic radius up to 200 nm at approximately 50 °C followed by a significant drop to 50 nm. This behavior has been seen for different thermosensitive polymers such as glycogen-*graft*-poly(2-alkyl-2-oxazolines),[35] amphiphilic polyoxazolines,[6,10] thermoresponsive nanoparticles based on poly(2-alkyl-2-oxazolines) and Pluronic F127,[7]

PNIPAM-*g*-PEO,[36] and poly(vinyl methyl ether).[37] The growth of nanoparticle size can be explained by the increasing aggregation number of formed nanoparticles. At elevated temperatures, above 50 °C, nanoparticles shrink with increasing of temperature due to worsening of the thermodynamic quality of the solvent.

3D-DLS experiments were conducted to obtain further information on size and dynamics of the nanoparticles and to investigate how apparent R_h is changing with increasing concentration at 40 °C. The intensity autocorrelation functions were fitted by double stretched exponential function $\left(A_1 \exp\left(-\left(\frac{t}{\tau_1}\right)^{\beta_1}\right) + A_2 \exp\left(-\left(\frac{t}{\tau_2}\right)^{\beta_2}\right) + B\right)$ from where the values of relaxation times were extracted (Figure 3A). Stretching parameters β_1 and β_2 describe polydispersity for each mode. The possible range for the β value lasts from 0 (high polydispersity) to 1, for an ideal monodisperse case. Experiments were conducted in a broad range of scattering angles, corresponding to scattering wave vectors q^2 from 0.5 × 10^{10} to 5.8 × 10^{10} cm^{-2}. In the vast majority of cases, the obtained values for the amplitude for the second mode (A_2) were negligible (below 0.005). That finding together with chaotic changes of polydispersity parameter β_2 as a function of angle, sometimes even above 1, led us to the conclusion to discard the second mode from consideration. For the β_1 parameter, we have observed monotonous dependence in a range of 0.95−1.0 that indicates low polydispersity of nanoparticles (Figure 3B, inset). The reverse relaxation times plotted for the fast mode (τ_1) as a function of q^2 indicate a diffusive nature of the relaxation process (Figure 3B) since $\frac{1}{\tau} = D_{app}q^2$ (ref 26). The values of apparent diffusion coefficients were calculated from the slope that were later depicted as a function of concentration (Figure 3C). From true values of diffusion coefficients calculated by extrapolation to infinite dilution, the true values of hydrodynamic radius were calculated for samples **A**, **C**, and **D**. These values were different from the ones measured by conventional DLS method (Figure 2). The discrepancy could be attributed to the fact that conventional DLS data were measured at finite concentration. It is known[38] that in a dilute regime the concentration dependence of a translation diffusion coefficient can be written as $D_t(c) = D_0(1 + k_D c)$. Here k_D is a second hydrodynamic virial coefficient which is specific to a particular polymer−solvent system and depends on a product of second virial coefficient and molecular weight $k_D = 2A_2M_w − k_f − \bar{v}$. Thus, the higher the molecular weights, the higher the k_D. Static light scattering supports the conclusion that the molecular weight of nanoparticles formed at 40 °C is very high (Table 2 and Supporting Information).

To get a deeper understanding of the internal structure of nanoparticles, NMR experiments were performed. The temperature dependence of a phase-separated fraction p, i.e., amount of polymer groups which take part in phase separation, was calculated for different groups (Figures 4 and 5). The p value calculated for the CH$_2$ of PNIPAM backbone shows different behavior as a function of temperature for PNIPAM and PNIPAM-*b*-PEG-*b*-PNIPAM copolymers (Figure 4). Whereas for PNIPAM, p reaches its highest value in a very narrow temperature range, all copolymers have a much broader transition. Microphase separation for PNIPAM-*b*-PEG-*b*-PNIPAM copolymers is complex: a sharp increase is followed by gradual growth. For **C** (PNIPAM$_{54}$-*b*-PEG$_{79}$(D)-*b*-PNI-
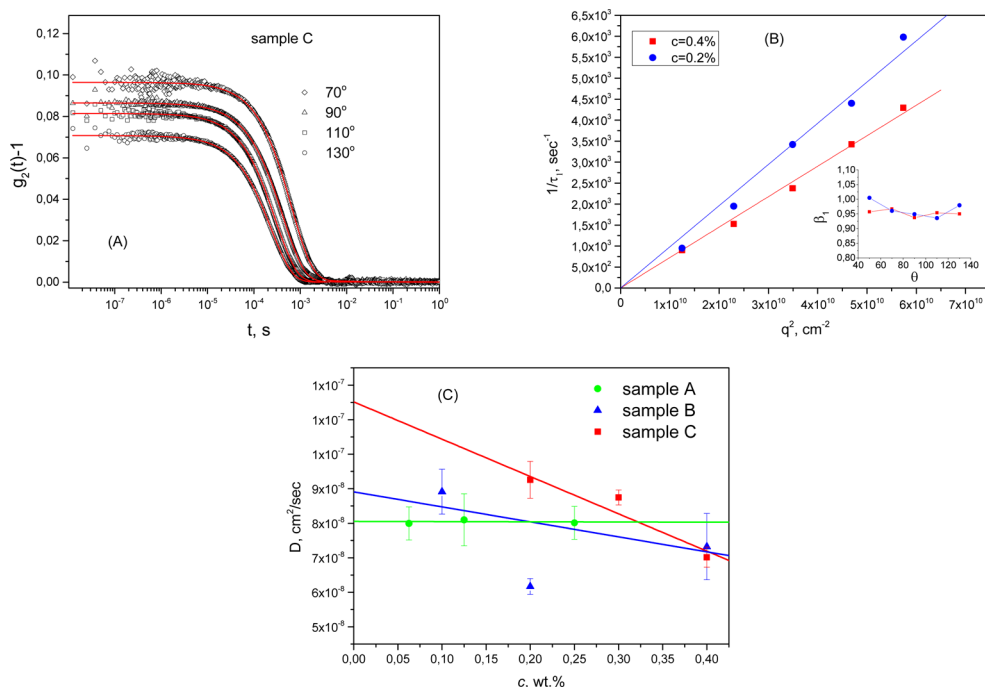
Figure 3. (A) Intensity autocorrelation functions for sample **C** at different angles measured by 3D-DLS method T = 40 °C, c = 0.4 wt % (B) q^2 dependence of the inverse relaxation time of the fast mode (τ_1) for sample **C**. Inset: angle dependence of the stretching parameter β_1. (C) Concentration dependence of apparent diffusion coefficients from 3D-DLS experiments for the fast mode (τ_1).

Table 2. Molecular Weight, Radius of Gyration, and Second Virial Coefficient of Nanoparticles at T = 40 °C Measured by SLS

	SLS			
	A	B	C	D
M_w, 10^6, Da	8.6	5.8	28	42
R_g, nm	106	107	137	124
A_2, 10^{-9} mol·dm³/g	−4.3	2.3	0.09	−0.72

Figure 5. Temperature dependence of the p-fraction as determined from integrated intensities of PEG chains for block copolymer **B** and block copolymer **D** from ^{1}H NMR spectra.

PAM$_{54}$) and **D** (PNIPAM$_{51}$-b-PEG$_{90}$-b-PNIPAM$_{51}$), a first stage of transition takes place at 30−47 °C, with the second one at 47−60 °C (Figure 4A). For the backbone of block copolymers **A** (PNIPAM$_{30}$-b-PEG$_{79}$(D)-b-PNIPAM$_{30}$) and **B** (PNIPAM$_{38}$-b-PEG$_{90}$-b-PNIPAM$_{38}$), the first stage occurs at 30−57 °C, the second one at 57−60 °C.

A comparison of p values for the backbone and pendant groups shows that the main chain of all copolymers participates fully in phase separati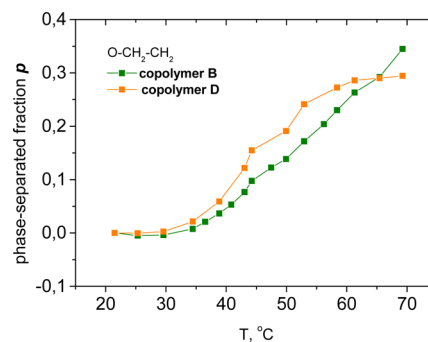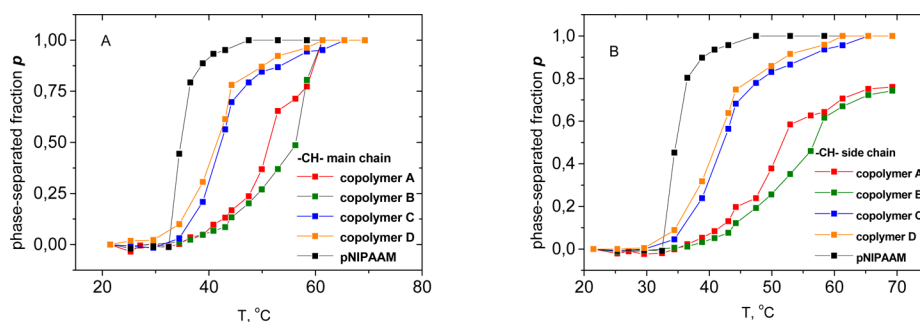on, while the pendant groups of copolymers **A** and **B** collapse to the globule on 75% (Figure 4B). Nevertheless, for copolymers with longer PNIPAM chains,

Figure 4. (A) Temperature dependence of the p-fraction as determined from integrated intensities of CH$_2$ band in ^{1}H NMR spectra of PNIPAM backbone. (B) Temperature dependence of the p-fraction as determined from integrated intensities of CH band in ^{1}H NMR spectra of PNIPAM pendant group.

Table 3. ¹H Spin−Spin Relaxation Times T₂ of CH₃ Protons of a Pendant Group of PNIPAM, HDO Molecules, and CH₂ Protons of PEG in D₂O Solutions of PNIPAM-b-PEG-b-PNIPAM Triblock copolymers

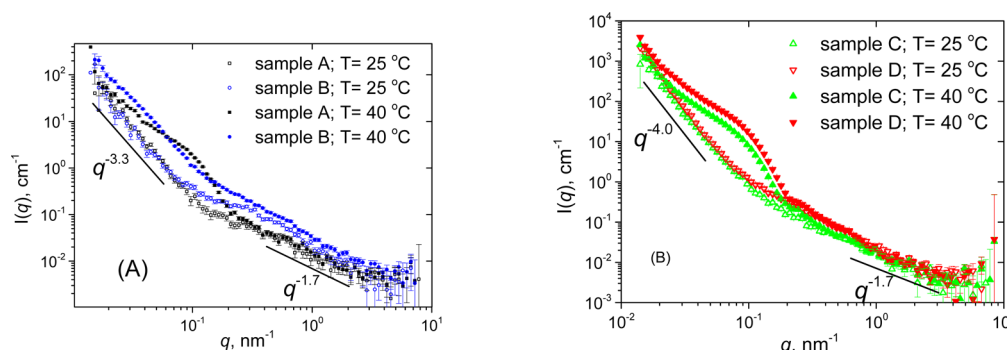| T, °C	PNIPAM (s)				HDO (s)				PEG (s)			
	A	B	C	D	A	B	C	D	A	B	C	D
22	0.16	0.166	0.14	0.13	7.56	2.26	3.04	3.13	0.55	0.51	0.56	0.51
67	0.25	0.329	0.71	0.24	4.72	4.28	2.90	3.00	1.17	0.91	1.05	0.76

Figure 6. SANS data for PNIPAM-b-PEG-b-PNIPAM copolymers at 25 and 40 °C. (A) block copolymers **A** and **B** and (B) block copolymers **C** and **D**.

Table 4. Fitting Parameters for Copolymers at 25 °C

	A	B	C	D
form factor: generalized Gaussian coil				
R_g^c, nm	3.5 ± 0.1	4.3 ± 0.3	2.1 ± 0.1	4.8 ± 0.1
ν	0.8 ± 0.2	0.58 ± 0.07	0.6 ± 0.2	0.62 ± 0.08
I_0^s, cm^{-1}	0.06 ± 0.01	0.17 ± 0.01	0.04 ± 0.01	0.19 ± 0.02
mass fractal form factor				
R_g^a, nm	66.7 ± 0.1	97.5 ± 0.1	105.0 ± 0.1	105.8 ± 0.1
D	2.58 ± 0.02	2.51 ± 0.02	2.75 ± 0.01	2.78 ± 0.01
I_0^a, cm^{-1}	34.4 ± 0.1	82.9 ± 0.1	1170 ± 1	1832 ± 1

C and **D**, the p value at high temperatures shows complete phase separation for pendant groups.

Interestingly, PEG chains also participate in the phase-separation process (Figure 5). With increasing temperature, up to 30% of PEG groups were involved in phase separation. For the copolymers with longer PNIPAM block (**C** and **D**), the phase separation parameter for PEG groups is higher.

The local mobility data obtained from NMR experiments are in agreement with conclusions based on p value. Below the CPT, PEG chains are very mobile and T₂ relaxation time is not influenced by the presence of the different terminal PNIPAM blocks (Table 3). It is known that ¹H spin−spin relaxation time T₂ of a specific group is proportional to its mobility, and therefore PNIPAM chains are obviously much slower than PEG below CPT. The same conclusion is valid for the case above the CPT, where the similar difference between the relaxation times of PEG and PNIPAM was observed. Here it should be noted that T₂ values reported in Table 3 for PNIPAM at 67 °C correspond only to a small fraction of groups that are still mobile and not involved in phase separation.

SANS. SANS experiments were conducted at 25 °C (below CPT) and 40 °C (above CPT). The experimental curves for all four samples are presented in Figure 6. The behavior of scattering curves at 25 °C was examined first and shows two features: a significant upturn at low $q < 0.2$ nm^{-1} and smooth decrease at $0.2 < q < 0.8$ nm^{-1}. The scattered intensity for the first region for samples **A** and **B** at $q < 0.2$ nm^{-1} obeys a power low with $I \sim q^{-3.3}$ that corresponds to structures with a loose

surface (Figure 6A). Scaterrers in samples **C** and **D** have sharp interface since they manifest classical Porod behavior $I \sim q^{-4.0}$ (Figure 6B). The same approach in a q range $q > 0.2$ nm^{-1} reveals power law of $I \sim q^{-1.7}$. This dependency is typical for Gaussian chains with excluded volume effects. Thus, it is possible to assume that the SANS curves below CPT contain the scattering from two different structures that could be fitted by a combination of two contributions, generalized Gaussian chain form factor and mass fractal form factor: $I(q) = P_{GGC}(q) + P_{MF}(q)$. The scattering function for the generalized Gaussian coil could be written as

$$P_{GGC}(q) = I_0^c \frac{U^{1/2\nu}\Gamma\left(\frac{1}{2\nu}\right) - \Gamma\left(\frac{1}{\nu}\right) - U^{1/2\nu}\Gamma\left(\frac{1}{2\nu}, U\right) + \Gamma\left(\frac{1}{\nu}, U\right)}{\nu U^{1/\nu}}$$

here, $U = (2\nu + 1)(2\nu + 2)\frac{q^2 R_g^2}{6}$ and $\Gamma\left(\frac{1}{2\nu}\right)$ is the gamma function.

The mass fractal form factor can be described as

$$P_{MF}(q) = 4\pi I_0^a \int_0^\infty r^{D-3} h(r, R) \frac{\sin(qr)}{qr} r^2 \, dr$$

where $h(r, R) = \exp\left[-\frac{Dr^2}{R_g^2}\right]$ is a cutoff function.

The choice of Gaussian chain form factor is obvious since we can expect such behavior for a single polymer chain below CPT. Concerning mass fractal contribution, there were several
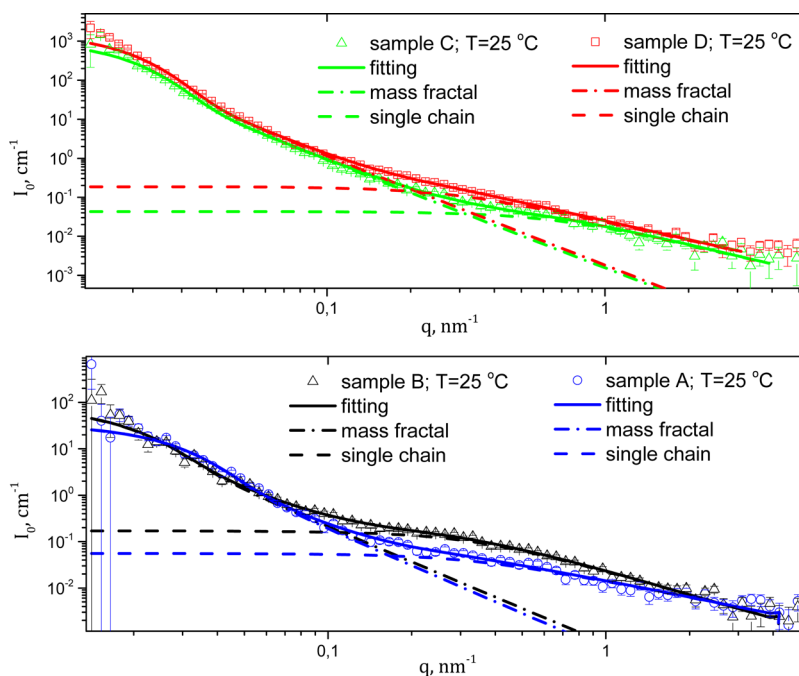
Figure 7. SANS data for polymers at 25 °C with results from the fitting procedure. Solid lines are fits.

models which plausibly describe scattering curves at $q < 0.2$ nm^{-1}, such as polydisperse hard spheres, fractal aggregates, and so forth; however, mass fractal contribution gave the best fitting results. The mass fractal contribution is attributed to a small fraction of aggregates observed by DLS. Six general parameters were used in the fitting procedure. Form factor: R_g^c, radius of gyration of chain; ν, excluded volume parameter or Flory exponent, and I_0^c, forward scattering of chain. Mass fractal form factor with parameters: I_0^a, forward scattering of fractal aggregates; R_g^a, radius of gyration of fractal aggregates; D, fractal dimension. Results from the fit of experimental curves are shown in Table 4 and Figure 7.

The data obtained from the fitting procedure with those that are coming from the description of chemical structure can now be compared. Several dependences could be pointed out. These features could be analyzed on different levels: on the level of single polymer chain, individual scatterers or entire particles. We shall begin our consideration with the level of polymer chain. While for the low molecular weight polymers (**A** and **B**, roughly 10−12 kDa), the variation in the length of thermoresponsive and hydrophilic block does not have significant effect on the gyration radius of single polymer chain, and the opposite was observed when molecular weight of polymer exceed 15 kDa (**C** and **D**). Thus, if we take the dimension of low molecular weight polymers as a reference, it becomes clear that the increase in the length of thermoresponsive block results in the formation of a more compact structure, even at temperature below the transition point. On the contrary, the increase in the length of hydrophilic block leads to a growth in the dimensions of polymer chain. The Flory exponent value of around 0.6 obtained from generalized Gaussian coil model for all polymers can be attributed to a swollen conformation of the polymer chain; water is a thermodynamically good solvent for our solutions at that particular temperature. Another feature appears when we compare the radius of individual scatterers from the structure factor with the corresponding radius of gyration of polymer

chain from the form factor (Table 4). While these values are close to each other for polymers **C** and **D**, the values from structure factor for polymers **A** and **B** exceed the values from form factor at least in two times. One can assume, the excluded volume has to be taken into account when the polymers **A** and **B** are analyzed. Interestingly, the inverse correlation occurred, if we compare the content of PNIPAM groups in polymer with dimension of individual scatters taken from the fitting results. The longer the PNIPAM block is, the smaller size of single scatter was determined. At the same time, on the level of whole particle, there is a well-defined relation between number of PEG units and dimension of whole aggregate. The increase in the length of PEG block results in increase in the size of entire aggregates. These aggregates are characterized by 2.5−2.7 fractal dimension that corresponds to the loose cluster objects.

If we apply the same strategy to the analysis of scattering curves recorded at 40 °C, one more feature should be considered in the interpretation of the experimental data: the shoulder appears at $0.03 < q < 0.2$ nm^{-1}. This shoulder is visible for every polymer and can be analyzed as a result of the transition process from a molecular state of polymer at 25 °C to an aggregate state at 40 °C. It has to be mentioned, the appearance of this shoulder in the scattering curve diminishes partly the first region, where the significant decrease in intensity was observed recently for curves at 25 °C, but it is still detectable at $q < 0.03$ nm^{-1}. Thus, there are three distinct regions here: $q < 0.03$ nm^{-1}, $0.03 < q < 0.2$ nm^{-1}, and $q > 0.2$ nm^{-1}. Application of the power law in this case gives the following results: $I_0 \sim q^{-1.4}$ for $q > 0.2$ nm^{-1}. Definition of the power law at values of q less than 0.03 nm^{-1} is complicated by the presence of only a few points in the region. Therefore, one can conclude that we are dealing with a very similar system. The only differences are a more compact sphere and stretched polymer chains in this particular case. For the purpose of quantitative analysis several different models have been tried for fitting. All of these models were a combination of certain form factor with MassFractal structure factor. Among form factors
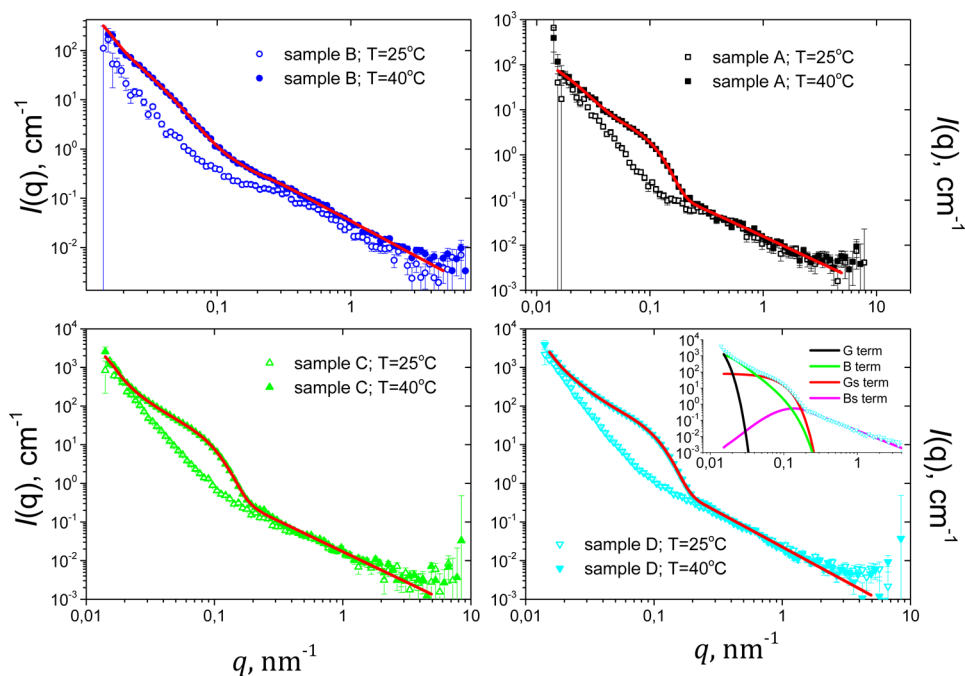
Figure 8. SANS data for every single polymer at 25 and 40 °C. Solid red lines are fits by the Beucage model. Inset for sample **D**: separated contributions according to the Beucage model.

Table 5. Fitting Parameters for Copolymers at 40 °C

fitting parameter of Beucage model	A, d-PEG	B, h-PEG	C, d-PEG	D, h-PEG
G	278	2061	15 057	58 845
B	$(1.2 \pm 1.0) \times 10^{-4}$	$(1.30 \pm 0.05) \times 10^{-2}$	$(4 \pm 1) \times 10^{-3}$	$(3.5 \pm 0.1) \times 10^{-3}$
G_s	6.2 ± 0.2	1.60 ± 0.03	40.2 ± 0.2	80.18 ± 0.01
B_s	$(1.6 \pm 0.1) \times 10^{-2}$	$(3.5 \pm 0.1) \times 10^{-2}$	$(1.7 \pm 0.1) \times 10^{-2}$	$(2.3 \pm 0.1) \times 10^{-2}$
R_{LS}, nm	156.5 ± 0.2	203.9 ± 0.1	184.6 ± 0.1	221.5 ± 0.1
R_{sub}, nm	20 ± 1	25.17 ± 0.01	14.54 ± 0.04	16.9 ± 0.1
R_s, nm	19.5	15.88 ± 0.02	24.27 ± 0.02	22.8 ± 0.1
D	3.4 ± 0.1	2.3 ± 0.1	2.9 ± 0.1	3.15 ± 0.02
D_s	1.17 ± 0.03	1.46 ± 0.01	1.58 ± 0.04	1.80 ± 0.03
χ^2	67.9	69.4	98.6	106.7

which were applied, i.e., hard sphere, generalized Gaussian coil, sphere with exponential shell, sphere with attached Gaussian chains, Dozier model, and the Beucage model. The only model that was successful in describing the behavior of scattering curves was the Beucage mode[39] (Figure 8 and Table 5).

The Beucage model describes fractal aggregates consisting of smaller particles:

$$I_{BC}(q) = G \exp\left(-\frac{q^2 R_{LS}^2}{3}\right) + B \exp\left(-\frac{q^2 R_{sub}^2}{3}\right)$$
$$\times \left(\frac{[\mathrm{erf}(qR_s/\sqrt{6})]^3}{q}\right)^D + G_s \exp\left(-\frac{q^2 R_s^2}{3}\right)$$
$$+ B_s \left(\frac{[\mathrm{erf}(qR_s/\sqrt{6})]^3}{q}\right)^{D_s}$$

The fitting parameters for the model are G, the Guinier prefactor of the larger structure; B, a prefactor specific to the type of power-law scattering; G_s, the Guinier prefactor of the smaller structure; B_s, a prefactor specific to the type of power-law scattering; R_{LS}, large-scale structure; R_{sub}, surface-fractal cutoff radius of gyration; R_s, size of small subunits; D, scaling exponent of the power law assigned to the larger structure R_g; D_s, scaling exponent of the power law assigned to the smaller structure R_s.

There are nine fitting parameters in the Beucage model described above, and while all values obtained from the fitting procedure are rationalizable, we cannot completely exclude the possibility that another model could also describe the SANS data. This hypothetical model should have a similar hierarchical structure, in order to describe such a complex system.

At 40 °C, nanoparticles made of copolymers **A** and **C** have overall radius of 156 and 185 nm, respectively, consisting of small 20.3 and 14.5 nm particles that are arranged inside of a fractal with scaling power laws 3.36 and 2.89 (surface fractal). Inside of the small particles, they behave as polymers with some excluded volumes effect (scaling power laws are 1.17 and 1.58) (Figure 9). Nanoparticles made of copolymers **B** and **D** are somewhat bigger than the ones composed of **A** and **C** due to protonated PEG.

NMR, DLS, and SANS data together provide an opportunity to describe nanoparticles formation in detail. Below CPT, triblock copolymers exist in solution as single molecules together with a small fraction of large aggregates as it is nicely
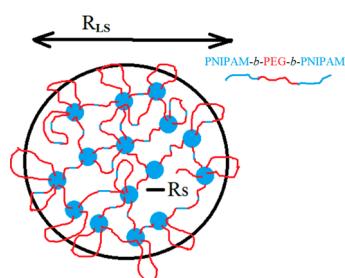
Figure 9. Hypothetical structure of nanoparticles above CPT.

seen by DLS and SANS. Analysis of T_2 data from NMR shows that PNIPAM blocks are less mobile in comparison with a middle PEG block. Formation of nanoparticles starts from occurrence of small domains formed by PNIPAM blocks since they disappear from the NMR spectrum. In contrast with pure PNIPAM, nanoparticle formation for PNIPAM-*b*-PEG-*b*-PNIPAM expands over a broader temperature range and such broadening depends on the length of PEG chain. *p*-Fraction value extracted from NMR data proves that mobile PEG chains significantly retard fast phase separation process. Nevertheless, at temperature much higher than CPT, up to 100% of all PNIPAM monomers could be inside of domains. The overall structure of nanoparticles formed above CPT could be described on a large scale as a surface fractal structure. PNIPAM domains were visualized by SANS contrast variation study by using deuterated PEG block.

CONCLUSIONS

For the first time, the onset of nanoparticle formation above CPT of PNIPAM-*b*-PEG-*b*-PNIPAM block copolymers has been analyzed in aqueous solutions in depth. The findings can be summarized as follows: Below CPT, triblock copolymers exist in solution as single molecules together with a small fraction of large aggregates. PNIPAM blocks are less mobile in comparison with a middle PEG block. Formation of nanoparticles with hierarchical structure was observed above CPT. The nanoparticles could be described on a large scale as a surface fractal structure. On a short scale, nanoparticles consist of small domains of partially phase-separated PNIPAM blocks interconnected by mobile PEG chains. Such domains were visualized by SANS contrast variation study by using deuterated PEG block. Further increase in temperature above CPT leads to higher immobilization of PNIPAM blocks inside of domains up to 100% of all monomer units.

ASSOCIATED CONTENT

Ⓢ Supporting Information

The Supporting Information is available free of charge on the ACS Publications website at DOI: 10.1021/acs.langmuir.6b00284.

> Synthesis of PEG macroinitiator; synthesis of ME$_6$TREN; Guinier plot for sample **C**; Guinier plot for sample **B**, temperature 40 °C; Guinier plot for sample **D**, temperature 40 °C (PDF)

AUTHOR INFORMATION

Corresponding Authors

*Tel: +420-608720561. Fax: +420-296809410. E-mail: sfill225@gmail.com.

*Tel: +44 (0)170 728 3439. E-mail: m.cook5@herts.ac.uk.

Author Contributions

The manuscript was written through contributions of all authors. All authors have given approval to the final version of the manuscript.

Notes

The authors declare no competing financial interest.

REFERENCES

(1) Aseyev, V.; Tenhu, H.; Winnik, F. M. Non-ionic Thermoresponsive Polymers in Water. *Adv. Polym. Sci.* **2010**, *242*, 29−89.

(2) Wang, X.; Wu, C. Light-Scattering Study of Coil-to-Globule Transition of a Poly(N-isopropylacrylamide) Chain in Deuterated Water. *Macromolecules* **1999**, *32*, 4299−4301.

(3) Prabaharan, M.; Grailer, J. J.; Steeber, D. A.; Gong, S. Q. Thermosensitive micelles based on folate-conjugated poly(N-vinyl-caprolactam)-block-poly(ethylene glycol) for tumor-targeted drug delivery. *Macromol. Biosci.* **2009**, *9*, 744−753.

(4) Hruby, M.; Konak, C.; Kucka, J.; Vetrik, M.; Filippov, S. K.; Vetvicka, D.; Mackova, H.; Karlsson, G.; Edwards, K.; Rihova, B.; Ulbrich, K. Thermoresponsive, Hydrolytically Degradable Polymer Micelles Intended for Radionuclide Delivery. *Macromol. Biosci.* **2009**, *9*, 1016−1027.

(5) Hruby, M.; Filippov, S. K.; Panek, J.; Novakova, M.; Mackova, H.; Kucka, J.; Ulbrich, K. Thermoresponsive micelles for radionuclide delivery. *J. Controlled Release* **2010**, *148*, E60−E62.

(6) Hruby, M.; Filippov, S. K.; Panek, J.; Novakova, M.; Mackova, H.; Kucka, J.; Vetvicka, D.; Ulbrich, K. Polyoxazoline Thermoresponsive Micelles as Radionuclide Delivery Systems. *Macromol. Biosci.* **2010**, *10*, 916−924.

(7) Panek, J.; Filippov, S. K.; Hruby, M.; Rabyk, M.; Bogomolova, A.; Kucka, J.; Stepanek, P. Thermoresponsive Nanoparticles Based on Poly(2-alkyl-2-Oxazolines) and Pluronic F127. *Macromol. Rapid Commun.* **2012**, *33*, 1683−1689.

(8) Bogomolova, A.; Hruby, M.; Panek, J.; Rabyk, M.; Turner, S.; Bals, S.; Steinhart, M.; Zhigunov, A.; Sedlacek, O.; Stepanek, P.; Filippov, S. K. Small-angle X-ray scattering and light scattering study of hybrid nanoparticles composed of thermoresponsive triblock copolymer F127 and thermoresponsive statistical polyoxazolines with hydrophobic moieties. *J. Appl. Crystallogr.* **2013**, *46*, 1690−1698.

(9) Laga, R.; Janouškova, O.; Ulbrich, K.; Pola, R.; Blazkova, J.; Filippov, S. K.; Etrych, T.; Pechar, M. Thermo-responsive polymer micelles as nano-sized pharmaceuticals for cancer therapy. *Biomacromolecules* **2015**, *16*, 2493−2505.

(10) Bogomolova, A.; Filippov, S. K.; Starovoytova, L.; Angelov, B.; Konarev, P.; Sedlacek, O.; Hruby, M.; Stepanek, P. Study of Study of Thermosensitive Amphiphilic Poly-Oxazolines of Complex Nature and Their Interaction with Ionic Surfactants. Hydrophobic, Thermosensitive and Hydrophilic Moieties: Are They Equally Important? *J. Phys. Chem. B* **2014**, *118*, 4940−4950.

(11) Duval, M.; Waton, G.; Schosseler, F. Temperature-induced growth of wormlike copolymer micelles. *Langmuir* **2005**, *21*, 4904−4911.

(12) Escobar-Chávez, J. J.; López-Cervantes, M.; Naïk, A.; Kalia, Y. N.; Quintanar-Guerrero, D.; Ganem-Quintanar, A. Applications of thermo-reversible pluronic F-127 gels in pharmaceutical formulations. *J. Pharm. Pharm. Sci.* **2006**, *9*, 339−358.

(13) He, C.; Kim, S. W.; Lee, D. S. In situ gelling stimuli-sensitive block copolymer hydrogels for drug delivery. *J. Controlled Release* **2008**, *127*, 189−207.

(14) Hoogenboom, R.; Thijs, H. M. L.; Jochems, M. J. H. C.; van Lankvelt, B. M.; Fijten, M. W. M.; Schubert, U. S. Tuning the LCST of poly(2-oxazoline)s by varying composition and molecular weight: alternatives to poly(N-isopropylacrylamide)? *Chem. Commun. (Cambridge, U. K.)* **2008**, 5758−5760.

(15) Topp, M. D. C.; Dijkstra, P. J.; Talsma, H.; Feijen, J. Thermosensitive Micelle-Forming Block Copolymers of Poly(ethylene glycol) and Poly(N-isopropylacrylamide). *Macromolecules* **1997**, *30*, 8518−8520.

(16) Virtanen, J.; Holappa, S.; Lemmetyinen, H.; Tenhu, H. Aggregation in Aqueous Poly(N-isopropylacrylamide)-block-poly-(ethylene oxide) Solutions Studied by Fluorescence Spectroscopy and Light Scattering. *Macromolecules* **2002**, *35*, 4763−4769.

(17) Zhu, P. Particle formation and aggregation - collapse behavior of poly (N -isopropylacrylamide) and poly (ethylene glycol) block copolymers in the presence of cross-linking agent. *J. Mater. Sci.: Mater. Med.* **2004**, *15*, 567−573.

(18) Zhang, W.; Shi, L.; Wu, K.; An, Y. Thermoresponsive Micellization of Poly (ethylene glycol)-b -poly (N-isopropylacrylamide) in Water. *Macromolecules* **2005**, *38*, 5743−5747.

(19) Zhao, J.; Zhang, G.; Pispas, S. Morphological transitions in aggregates of thermosensitive poly(ethylene oxide)-b-poly(N-isopropylacrylamide) block copolymers prepared via RAFT polymerization. *J. Polym. Sci., Part A: Polym. Chem.* **2009**, *47*, 4099−4110.

(20) Papagiannopoulos, A.; Zhao, J.; Zhang, G.; Pispas, S.; Radulescu, A. Thermoresponsive transition of a PEO-b-PNIPAM copolymer: From hierarchical aggregates to well defined ellipsoidal vesicles. *Polymer* **2013**, *54*, 6373−6380.

(21) Lin, H. H.; Cheng, Y. L. In-situ thermoreversible gelation of block and star copolymers of poly(ethylene glycol) and poly(n-isopropylacrylamide) of varying architectures. *Macromolecules* **2001**, *34*, 3710−3715.

(22) Teodorescu, M.; Negru, I.; Stanescu, P. O.; Draghici, C.; Lungu, A.; Sarbu, A.c Thermogelation properties of poly(N-isopropylacryla-mide) − block − poly(ethylene glycol) − block − poly(N-isopropylacrylamide) triblock copolymer aqueous solutions. *React. Funct. Polym.* **2010**, *70*, 790−797.

(23) De Graaf, A. J.; Boere, K. W.; Kemmink, J.; Fokkink, R. G.; van Nostrum, C. F.; Rijkers, D. T.; van der Gucht, J.; Wienk, H.; Baldus, M.; Mastrobattista, E.; Vermonden, T.; Hennink, W. E. Looped structure of flowerlike micelles revealed by 1H NMR relaxometry and light scattering. *Langmuir* **2011**, *27*, 9843−9848.

(24) Radecki, M.; Spěváček, J.; Zhigunov, A.; Sedláková, Z.; Hanyková, L. Temperature-induced phase transition in hydrogels of interpenetrating networks of poly(N-isopropylacrylamide) and poly-acrylamide. *Eur. Polym. J.* **2015**, *68*, 68−79.

(25) Kourilova, H.; Čťastná, J.; Nyková, L.; Dláková, Z.; Spěváček, J. ¹H NMR study of temperature-induced phase separation in solutions of poly(N-isopropylmethacrylamide-co-acrylamide) copolymers. *Eur. Polym. J.* **2010**, *46*, 1299−1306.

(26) Spěváček, J. NMR investigations of phase transition in aqueous polymer solutions and gels. *Curr. Opin. Colloid Interface Sci.* **2009**, *14*, 184−191.

(27) http://www.mantidproject.org/Main_Page.

(28) Wignall, G. D.; Bates, F. S. Absolute calibration of small-angle neutron scattering data. *J. Appl. Crystallogr.* **1987**, *20*, 28−40.

(29) Pecora, R. *Dynamic Light Scattering: Applications of Photon Correlation Spectroscopy*; Plenum Press: New York, 1985.

(30) Chu, B. *Laser Light Scattering: Basic Principles and Practice*; Academic Press, Inc.: New York, 1991.

(31) Urban, C.; Schurtenberger, P. Characterization of turbid colloidal suspensions using light scattering techniques combined with cross-correlation methods. *J. Colloid Interface Sci.* **1998**, *207*, 150−158.

(32) Scheffold, F.; Schurtenberger, P. Light scattering probes of viscoelastic fluids and solids. *Soft Mater.* **2003**, *1*, 139−165.

(33) Pusey, P. N. Suppression of multiple scattering by photon cross-correlation techniques. *Curr. Opin. Colloid Interface Sci.* **1999**, *4*, 177−185.

(34) Ye, J.; Narain, R. Water-assisted atom transfer radical polymerization of N-isopropylacrylamide: nature of solvent and temperature. *J. Phys. Chem. B* **2009**, *113*, 676−681.

(35) Pospisilova, A.; Filippov, S. F.; Bogomolova, A.; Turner, S.; Sedlacek, O.; Matushkin, N.; Cernochova, Z.; Stepanek, P.; Hruby, M. Glycogen-graft-poly(2-alkyl-2-oxazolines) − the new versatile biopol-ymer-based thermoresponsive macromolecular toolbox. *RSC Adv.* **2014**, *4*, 61580−61588.

(36) Virtanen, J.; Baron, C.; Tenhu, H. Grafting of poly(N-isopropylacrylamide) with poly(ethylene oxide) under various reaction conditions. *Macromolecules* **2000**, *33*, 336−341.

(37) Aseyev, V.; Hietala, S.; Laukkanen, A.; Nuopponen, M.; Confortini, O.; Du Prez, F. E.; Tenhu, H. Mesoglobules of thermoresponsive polymers in dilute aqueous solutions above the LCST. *Polymer* **2005**, *46*, 7118−7131.

(38) Yamakawa, H. *Modern Theory of Polymer Solutions*; Harper and Row: New York, 1971.

(39) Beaucage, G. Approximations leading to a unified exponential/power-law approach to small-angle scattering. *J. Appl. Crystallogr.* **1995**, *28*, 717−728.